Chinese Journal of
POLYMER SCIENCE

RESEARCH ARTICLE

https://doi.org/10.1007/s10118-026-3705-7
Chinese J. Polym. Sci.

Sequence-encoded Conformation Pathways in Viscoelastic Microphase Separation of Multiblock Copolymers

Zhe-Peng Zhu, Jia-Ping Lin, and Liang-Shun Zhang*

Shanghai Key Laboratory of Advanced Polymeric Materials, School of Materials Science and Engineering, East China University of Science and Technology, Shanghai 200237, China

Electronic Supplementary Information

Abstract Deciphering how molecular sequences of block copolymers program their self-assembly pathways is a pivotal pursuit in polymer science. To this end, we integrated viscoelastic constitutive relations into dynamic self-consistent field theory (DSCFT) to probe the spatiotemporally coupled evolution of nanostructures and chain conformations in sequence-defined multiblock copolymers during viscoelastic microphase separation. The DSCFT simulations reveal that the linear sequence of slow-relaxing "hard" and fast-relaxing "soft" blocks encodes two programmable kinetic motifs: a hard-soft-hard sequence drives a sharp, droplet-coalescence-triggered conversion from loop to bridge conformations during viscoelasticity-mediated phase inversion, whereas a soft-hard-soft sequence governs a gradual, network-contraction-driven relaxation of chain conformations. Serving as modular kinetic codes identified in the system of triblock copolymers, these kinetic motifs were shown to operate concurrently within tetrablock chains and generalize to penta- and hexa-block architectures, demonstrating the scalability and robustness of sequence-encoded dynamics. This work establishes the paradigm of sequence-encoded viscoelastic kinetics, providing a mechanism for controlling pathway-dependent self-assembly at the molecular level.

Keywords Multiblock copolymers; Viscoelastic microphase separation; Dynamic self-consist field theory; Conformation dynamics; Sequence design

Citation: Zhu, Z. P.; Lin, J. P.; Zhang, L. S. Sequence-encoded conformation pathways in viscoelastic microphase separation of multiblock copolymers. *Chinese J. Polym. Sci.* https://doi.org/10.1007/s10118-026-3705-7

INTRODUCTION

The spatiotemporal organization of functional matter in living systems, spanning membraneless organelles to extracellular matrices, is rooted in liquid-liquid phase separation.[1–7] The pathways and outcomes of this phase separation process are governed not only by thermodynamics but also by the sequence-encoded kinetic properties of proteins and RNAs.[8–12] These biomolecules can be viewed as natural multiblock copolymers, where specific linear sequences of cohesive "sticker" and flexible "spacer" motifs program both thermodynamic driving forces and a defined spectrum of relaxation dynamics.[13–16] This programmed disparity in relaxation timescales governs the formation of nonequilibrium structures, such as metastable condensates and transient networks.[17–23] Consequently, molecular sequence dictates both the thermodynamic landscape and the ordering kinetics of phase separation, ultimately specifying the chain conformations and higher-order structural organization within biomolecular assemblies.[24–26] Therefore, deciphering and emulating this sequence-encoded kinetics constitutes a central pursuit in polymer science, demanding a model system with precise architecture control.

Synthetic multiblock copolymers, with their precisely tunable sequence of chemically distinct blocks, provide an ideal platform to emulate biological programmability and decipher the physical code linking the sequence to self-assembly.[27–32] Their modular architecture allows for the systematic encoding of information not only through block chemistry but also through variables such as block number, length and topology. Theoretically, predictive tools, such as self-consistent field theory and coarse-grained simulations, have established how these parameters map to a vast landscape of equilibrium nanostructures.[33–45] Experimentally, systems ranging from PEO-based multiblock copolymers to elastin-like polypeptides have demonstrated the ability to precisely control their nanostructure and response properties through sequence design.[46–51] Collectively, these works have established a powerful thermodynamic design framework, enabling precise prediction and realization of equilibrium self-assembly outcomes. However, this static and endpoint-focused control contrasts with the dynamic and pathway-dependent kinetics essential for biological function.

To bridge this gap between static endpoint design and kinetic pathway control, the spectrum of relaxation dynamics encoded by a multiblock sequence emerges as the pivotal

* Corresponding author, E-mail: zhangls@ecust.edu.cn
Received March 11, 2026; Accepted April 7, 2026; Published online July 1, 2026

design dimension governing self-assembly kinetics. The linear sequence dictates the spatial arrangement of the slow-relaxing "hard" and fast-relaxing "soft" blocks.[52–56] This molecular-level disparity in relaxation timescales manifests macroscopically as viscoelastic asymmetry between distinct components. During phase separation as a typical example, such asymmetry fundamentally redirects morphological evolution away from classical pathways such as nucleation-growth or spinodal decomposition, driving the system into a distinct regime of viscoelastic phase separation (VPS).[57–61] In the VPS, the kinetic pathway of multicomponent polymers is dictated by a competition between the inherent relaxation time of distinct components and the characteristic deformation rate of demixing. This dynamic interplay suppresses normal diffusion coarsening and promotes the formation of non-equilibrium patterns, such as transient networks or sponge-like morphologies,[62–69] wherein the slower-relaxing hard blocks act as kinetic traps. Notably, this can lead to distinctive pathways, such as phase inversion, where the initial morphology inverts during VPS.

Building on the established role of dynamic asymmetry in the VPS, our recent work on diblock copolymers validated its capability to reprogram the kinetic pathways of self-assembly.[70] By incorporating viscoelastic constitutive relations into the dynamic self-consistent field theory (DSCFT),[71–75] we demonstrated that a pronounced disparity in bulk modulus can trigger composition-independent phase inversion, yielding metastable percolating networks. This finding confirms that dynamic asymmetry can bypass thermodynamic constraints, yet it immediately raises the pivotal and more complex question for sequence-defined polymers: how does the precise linear order of hard and soft blocks in multiblock copolymers deterministically encode non-equilibrium self-assembly pathways and, through these pathways, govern the spatiotemporal evolution of chain conformations (*e.g.*, bridging versus looping)?

To decode how the molecular sequence dictates both nanostructures and their dynamics, we employed viscoelastic DSCFT to investigate how the linear sequence of hard and soft blocks governs the selection of self-assembly pathways of multiblock copolymers in viscoelastic microphase separation (VμPS). This methodology integrates time-dependent stress relaxation with chain conformation dynamics, enabling spatiotemporally resolved simulations of coupled structure and conformation evolution. By designing a series of sequences with permutations of hard and soft blocks, we elucidated how specific sequences of different blocks program distinct kinetic pathways of self-assembly and direct the evolution of chain conformations. Furthermore, we probed the modularity and generality of these kinetic pathways by examining their concurrent operation within a single chain and transferability to longer sequences. This work bridges the gap between the static endpoint-focused paradigm of traditional thermodynamics and the dynamic pathway-dependent programming essential to biological functions.

THEORETICAL MODELLING AND COMPUTATIONAL METHODS

In this study, we extended the DSCFT to model the viscoelastic microphase separation of AB-type multiblock copolymers. With the evolving structures and external fields obtained from the DSCFT simulations, we calculated the statistical distribution of the chain conformations of AB-type multiblock copolymers. In the following, we briefly outline the key aspects of the DSCFT model.

We introduced a general parity-based principle to model a series of linear AB-type multiblock copolymers, where the overall composition (*i.e.*, overall volume fractions of blocks A and B, $f_A = f_B = 0.50$) was held constant, while the sequence symmetry and total number of blocks were varied. Based on this principle, two distinct families of multiblock copolymers have been constructed. The even-parity $(AB)_n$ series comprises chains with an even number of blocks and inherently dissimilar end-blocks. To isolate the architectural effect, a symmetric composition constraint was enforced (*i.e.*, each block had an identical volume fraction), thereby maximizing sequence symmetry and conformational freedom. The odd-parity $(AB)_nA$ series consists of chains with odd numbers of blocks and identical end blocks. Herein, the inversion symmetry of the composition and the overall composition balance are maintained by designing the two end A-blocks to have half the volume fraction of the internal blocks. To maintain this symmetry, we set the two end blocks as half the volume fraction of the internal blocks. This choice ensures that the overall molecular architecture is invariant under an end-to-end inversion. The architecture, sequence, and composition of the multiblock copolymers are schematically illustrated in Fig. S1 (in the electronic supplementary information, ESI).

Within the framework of the self-consistent field theory, we modeled AB-type multiblock copolymer systems as weakly compressible melts composed of Gaussian chains.[76] The connectivity of the polymers is described through harmonic constraints that account for chain elasticity and configuration entropy. The repulsive interactions between distinct A and B blocks are captured by the Flory-Huggins interaction parameter χ scaled by the degree N of polymerization. The system is represented using local volume fraction fields φ_A and φ_B as well as the conjugate chemical potential fields ω_A and ω_B. These fields satisfy a bijection relationship.[72,73]

The evolution of the local volume fraction fields φ_A and φ_B during VμPS is governed by the continuity equations within a two-fluid model.[74,75] Viscoelastic stresses arising from both shear and bulk relaxation mechanisms were modeled using an Oldroyd-B-type constitutive relation.[77] This model captures the time-dependent stress response through the interplay between the shear modulus $G_{I,0}$ (I = A and B) and bulk modulus $K_{I,0}$, all of which depend on φ_I. These material parameters describe the nonlinear viscoelastic behavior of a heterogeneous polymer system.

The DSCFT equations were solved using a multi-step numerical scheme.[78] All simulations were performed in two dimensions under periodic boundary conditions on a 128×128 lattice spanning a domain of $32R_g \times 32R_g$, where R_g denotes the radius of gyration of the copolymer chain. A time step of $\Delta t = 10^{-5}\tau$ was adopted, where τ is the characteristic diffusion time. The characteristic stress is given by $\sigma_c = \eta/\tau$, where η is the viscosity coefficient of distinct blocks. Each simulation started from a homogeneous state with small random fluctuations and five independent runs with different ran-

https://doi.org/10.1007/s10118-026-3705-7

dom seeds were performed for each parameter setting. Further details regarding the DSCFT model of the AB-type multiblock copolymers are provided in Section S1 (in ESI).

Based on the temporal profiles of the local volume fraction fields φ_I and conjugate fields ω_I obtained from the DSCFT simulations, we statistically analyzed the chain conformations of the AB-type multiblock copolymers to establish a quantitative connection between the molecular sequence and mesoscopic structures during VμPS. To this end, we extended the analysis of the equilibrium loop probability to our non-equilibrium system for sub-chains of linear AB-type multiblock copolymers.[79–81] The method begins by partitioning the system into Voronoi cells, each centered around a single I-rich (I = A or B) nanodomain by the thinning algorithm. An end block of the sub-chain is assigned to a cell if its A-B junction lies within the corresponding Voronoi region. We then focused on a representative cell to compute the loop probability using a modified propagator formalism, where the partition function is spatially restricted to the targeted nanodomain. This approach can evaluate the likelihood that the inner block of the sub-chain forms a loop conformation within the resident nanodomain. Given the statistical equivalence of all Voronoi cells, the overall loop probability f_{loop} of the sub-chain was obtained by spatial averaging.

Beyond chain-level statistics, we introduce two morphology-based metrics (*i.e.*, area fraction f_{area} and Euler characteristic χ_{Euler}) to characterize the evolving structures quantitatively. The local volume fraction threshold $\varphi_I > f_I$ was used to identify I-rich nanodomains. The area fraction f_{area} is defined as the ratio of the area occupied by the I-rich nanodomains to the total area of the system, reflecting the relative spatial coverage of the I-rich phase. The Euler characteristic χ_{Euler} derived from the interface genus captures the topological complexity and pore structure of nanodomains. For instance, $\chi_{Euler} \approx 0$ indicates continuous lamellae, whereas $\chi_{Euler} < 0$ indicates a perforated or network-like morphology.

RESULTS AND DISCUSSION

In our previous work,[70] DSCFT simulations were used to probe the VμPS of simple A_1B_1 diblock copolymers (corresponding to the n=1 case of the $(AB)_n$ series). It was demonstrated that the A_1B_1 system exhibits a unique pathway of microphase separation, where dispersed droplets are initially formed by low-module blocks and subsequently evolve into a lamellar structure (*i.e.*, a distinctive phase inversion phenomenon). This phenomenon highlights the governing role of viscoelastic mismatch in structural evolution. Extending from diblock to multiblock architectures introduces not only a greater conformational complexity but also a key new variable: the sequence order of blocks with different moduli. This sequence directly encodes the spatial arrangement of dynamic asymmetry along the chain, which is expected to couple strongly with the viscoelastic response and thereby regulate the non-equilibrium conformation pathway. To reveal the intricate interplay among viscoelasticity sequence, chain conformation, and microphase-separated structures, we now apply DSCFT simulations to investigate the VμPS behaviors of $(AB)_nA$ and $(AB)_n$ multiblock copolymers, focusing on how sequence-encoded dynamic asymmetry dictates both structural evolution and chain-level conformational changes.

In our model, dynamic asymmetry arises from a mismatch in the intrinsic dynamic properties, such as viscoelasticity between the constituent blocks. Given that the bulk modulus plays a dominant role in governing the resulting non-equilibrium pathway,[60,82] we focus on the disparity in the bulk modulus to introduce dynamic asymmetry. Herein, a component with a higher bulk modulus exhibits a more solid-like, elastic response and is designated as slow-relaxing "hard" block (H), whereas a component with a lower bulk modulus displays a more fluid-like character and is termed as fast-relaxing "soft" block (S). This difference in mechanical properties is quantified by the disparity in the bulk modulus, $\Delta K = K_{A,0} - K_{B,0}$. In the Oldroyd-B model, viscoelastic stress scales with the bulk moduli. Consequently, hard blocks generate higher stresses and relax more slowly (slower stress relaxation), whereas soft blocks generate lower stresses and relax faster (faster stress relaxation). To isolate the effect of dynamic asymmetry from the bulk modulus disparity, the shear moduli for both block types were set to be equal (*i.e.*, $G_{A,0} = G_{B,0} = \sigma_c$).

Viscoelastic Microphase Separation of Triblock Copolymers

We began by investigating the simplest odd-parity architecture, the $A_1B_1A_2$-type triblock copolymer, which corresponds to the case of $(AB)_nA$ with n = 1. For the symmetric triblock copolymer system, we constructed two distinct sequences, placing the hard and soft blocks: one with hard outer blocks and a soft inner block (denoted as $A_{1H}B_{1S}A_{2H}$) and the other with soft outer blocks and a hard inner block ($A_{1S}B_{1H}A_{2S}$). To ensure a symmetric chain architecture for both sequences, the total volume fraction of the A component was fixed at f_A=0.50, with two ampere blocks of equal length (f_{A1}=f_{A2}=0.25), and the inner B block thus had a volume fraction of f_B=0.50. The Flory-Huggins interaction parameter was set to $\chi N = 36$.

Focusing first on the $A_{1H}B_{1S}A_{2H}$ case, we examined how this specific arrangement of dynamic asymmetry directs the VμPS pathway. This sequence leads to a distinctive microphase separation pathway that markedly diverges from the behavior of its dynamically symmetric counterpart (Fig. S2 in ESI). As shown in the time-series snapshot in Fig. 1(a), the process of microphase separation begins with the rapid formation of a percolating network-like structure by the hard A_{1H} and A_{2H} blocks (t = 14τ), whereas the soft B_{1S} blocks are compressed and expelled into the isolated droplet-like domains embedded within this A-rich matrix. This is followed by a contraction of the percolating network (t = 20τ), accompanied by coarsening of the B-rich droplets. Such coarsening drives their coalescence (highlighted by red circles at t = 30τ), thereby forming irregular lamellar structures. Finally, these transient structures reorganized into randomly oriented lamellae (t = 180τ).

The morphological evolution of VμPS was quantitatively characterized by the time-dependent area fraction and topological metrics. Fig. 1(b) presents the temporal variation in the area fraction f_{area} of the B-rich nanodomains under different bulk modulus disparities ΔK. Under a dynamic symmetry of ΔK=0, f_{area} remains constant at 0.50. By contrast, under a dynamic asymmetry of $\Delta K = 8\sigma_c$ and $16\sigma_c$, f_{area} starts from a pronounced minimum and recovers toward 0.5. The corresponding temporal evolution of the Euler characteristic χ_{Euler} for B-

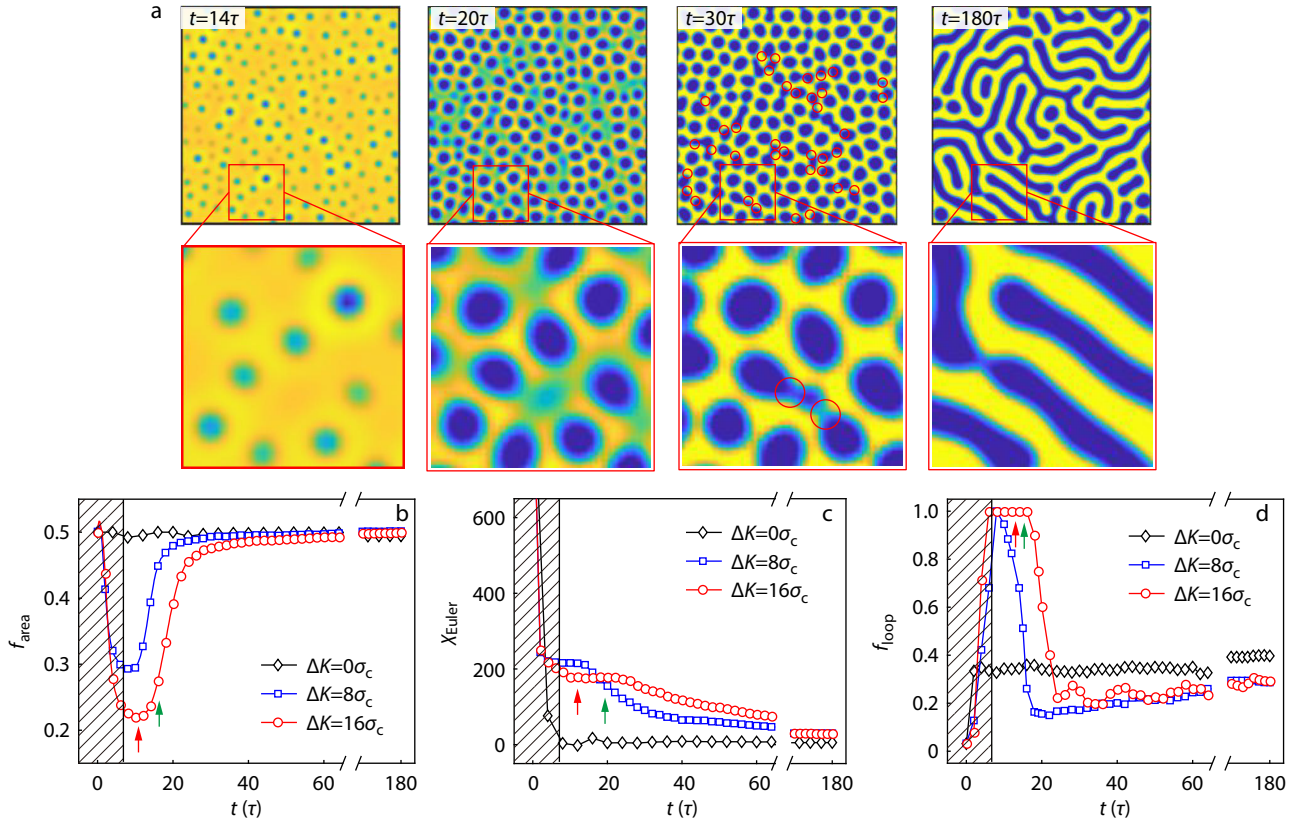

Fig. 1 (a) Morphological evolution of microphase-separated nanostructures of $A_{1H}B_{1S}A_{2H}$ triblock copolymers with higher bulk modulus of outer A blocks. The bulk modulus disparity between A and B blocks is set as $\Delta K = K_{A,0} - K_{B,0} = 16\sigma_c$. The A- and B-rich nanodomains are color-coded in yellow and blue, respectively. Note that all the profiles are displayed in the identical color map. Insets illustrate the enlarged images of local volume fraction field φ_A enclosed by dashed boxes. The red circles highlight the coalescence of B-rich domains. (b) Area fraction f_{area} and (c) Euler characteristic χ_{Euler} of B-rich nanodomains as a function the time t for triblock copolymers with tunable bulk modulus disparity ΔK. (d) Temporal change in loop probability f_{loop} of B_{1S} blocks. Error bars are omitted for clarity. Data from the early stage of microphase separation are excluded due to the lack of well-defined interfaces, as indicated by the shade area in Figs. 1(b)–1(d). The red and green arrows highlight the startups of phase inversion and conformation rearrangement for $\Delta K = 16\sigma_c$.

rich nanodomains is shown in Fig. 1(c). At $\Delta K = 0.0$, χ_{Euler} decreased monotonically to zero, which is consistent with the formation of randomly oriented lamellae. Under a dynamic asymmetry of $\Delta K > 0.0$, χ_{Euler} exhibits a distinct two-stage behavior. Taking $\Delta K = 16\sigma_c$ as an example, it remains nearly constant before $t = 20\tau$, indicating coarsening of the B-rich droplets without significant coalescence. After $t = 20\tau$, it declined toward zero, signifying the onset of fast coalescence and the final formation of lamellar structures. The recovery trajectories of f_{area} and χ_{Euler} from the extreme values clearly characterize the phase inversion phenomenon, the startup of which is marked by red arrows in Fig. 1.

Notably, beyond the phase inversion phenomenon, the triblock architecture with hard-outer/soft-inner sequence exhibits a unique conformation relaxation absent in the A_1B_1 diblock copolymers. This relaxation is directly captured by the temporal change in the loop probability f_{loop} of the B_{1S} blocks (Fig. 1d). The initial pronounced maximum in f_{loop} correlated with the formation of a percolating A-rich network, which forced the soft B_{1S} blocks into a loop conformation within the droplets. This is followed by an abrupt decline in f_{loop} at t-20τ (marked by the green arrow for $\Delta K = 16\sigma_c$), signifying a sudden conformational change driven by droplet coalescence during the phase inversion. Thereafter, f_{loop} gradually recovered as the system evolved into a lamellar structure. It should be mentioned that a smaller disparity in the bulk modulus accelerates the start-up of chain conformation rearrangement.

To elucidate the underlying mechanism during VμPS, we analyzed temporal changes in the thermodynamic force $\mathbf{F}_\varphi = -\sum_I \varphi_I \nabla \mu_I$ and viscoelastic forces $\mathbf{F}_I = -\nabla \cdot \boldsymbol{\sigma}_I$ acting on I-type blocks (Eqs. S9 and S10 in ESI). The spatially averaged magnitudes per lattice are given by $F_\varphi = |\mathbf{F}_\varphi|$ and $F_I = |\mathbf{F}_I|$ and are shown in Fig. 2(a). In the initial stage of phase inversion (*e.g.*, t-14τ), the modulus mismatch of incompatible A and B blocks generates asymmetry in the viscoelastic stresses. The higher viscoelastic force F_A of the harder A_{1H} and A_{2H} blocks promotes the formation of a percolating network, whereas the lower viscoelastic force F_B of the softer B_{1S} blocks allows them to yield compressed droplets. Thus, the B_{1S} blocks were forced into a loop conformation *via* elastic confinement within the A-rich matrix. Subsequently, the increasing influence of the thermodynamic force F_φ from the incompatibility of the A and B blocks accelerates the phase inversion process. Meanwhile, the viscoelastic forces accumulated and reached a peak at t-20τ. Their subsequent dissipation leads to the coalescence of B-rich droplets and rupture of the A-rich network.

https://doi.org/10.1007/s10118-026-3705-7

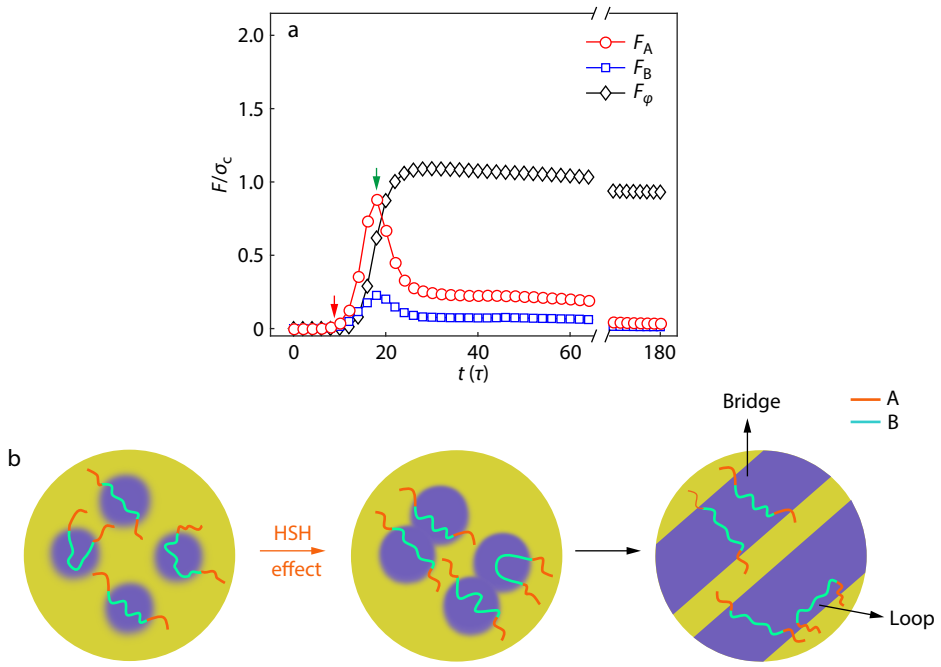

Fig. 2 (a) Time evolution in spatially averaged magnitudes of thermodynamic force $\mathbf{F}_\varphi$, viscoelastic force $\mathbf{F}_I$ of I-type blocks during the VμPS of $A_{1H}B_{1S}A_{2H}$ triblock copolymers. The bulk modulus disparity between A and B blocks is set as $\Delta K = K_{A,0} - K_{B,0} = 16\sigma_c$. The red and green arrows highlight the startups of phase inversion and conformation rearrangement. (b) Schematic of mechanistic pathway of hard-soft-hard (HSH) effect during coupled phase inversion and conformation rearrangement.

This structural reorganization was accompanied by conformational rearrangement of the B_{1S} blocks. Finally, as the viscoelastic forces continue to relax, the thermodynamic force drives the system toward a lamellar morphology.

Based on this analysis, we propose a mechanistic picture of the VμPS of the $A_{1H}B_{1S}A_{2H}$ triblock copolymers, as illustrated in Fig. 2(b). Initially, soft B-rich droplets were embedded within a percolating network of hard A_{1H} and A_{2H} blocks, resulting in a high loop probability for the B_{1S} blocks. As the viscoelastic forces relax, they facilitate the coarsening and coalescence of the B-rich droplets, which in turn triggers a pronounced conformation rearrangement, manifested as a sharp decrease in the loop probability f_{loop}. The system eventually relaxes into a lamellar morphology with the coexistence of the loop and bridge conformations. We term this distinctive kinetic pathway as hard-soft-hard (HSH) effect, revealing a mechanism absent in the microphase separation of conventional block copolymers.

Next, we examined the complementary case of triblock copolymers with a sequence of soft outer A blocks and a hard inner B block (*i.e.*, $A_{1S}B_{1H}A_{2S}$). This inverse dynamic asymmetry gives rise to a VμPS pathway that is morphologically and kinetically distinct from the $A_{1H}B_{1S}A_{2H}$ system. As shown in the morphological evolution (Fig. 3a) and the corresponding temporal profiles of the spatially averaged forces (Fig. S3 in ESI), the higher viscoelastic force of the hard inner B_{1H} blocks initially drives the formation of a swollen percolating network (highlighted by a double arrow), whereas the soft outer A_{1S} and A_{2S} blocks are compressed into isolated droplets (t = 14τ). Subsequently, the increasing influence of the thermodynamic force of incompatible A and B blocks causes the swollen B-rich network to contract and the A-rich droplets to coarsen (t = 20τ). Following a peak in the viscoelastic forces around t-20, their dissipation triggered the formation of irregular lamellar structures at t = 48τ. Ultimately, as the viscoelastic forces relax further, the thermodynamic force dictates the reorganization of these transient structures into randomly oriented lamellae (t = 180τ).

Quantitative analysis further highlighted the contrasting evolutionary pathways of the $A_{1H}B_{1S}A_{2H}$ and $A_{1S}B_{1H}A_{2S}$ systems. In the $A_{1S}B_{1H}A_{2S}$ system, the higher bulk modulus of the inner B blocks causes a decrease in the area fraction f_{area} of the B-rich nanodomains from its maximum at t = 14τ (Fig. 3b), reflecting the gradual contraction of the swollen B-rich network. In parallel, the Euler characteristic χ_{Euler} exhibited a sharp minimum at t = 14τ (Fig. 3c), quantitatively confirming the formation of a continuous B-rich network containing isolated A-rich droplets. The subsequent plateau in χ_{Euler} between t = 14τ and 20τ indicates that no rapid coalescence of A-rich droplets occurred during this stage. Thereafter, χ_{Euler} gradually approaches zero as the structure evolves toward the lamellar morphology.

In stark contrast to the $A_{1H}B_{1S}A_{2H}$ system, which exhibits a high initial loop probability f_{loop} ~ 1.0, the $A_{1S}B_{1H}A_{2S}$ triblock copolymers show a significantly reduction f_{loop} at about 0.6 for $\Delta K = 16\sigma_c$ (t = 14τ in Fig. 3d). This reduction in f_{loop} arises from the formation of a swollen B-rich percolating network, which increases the average distance between A-rich droplets. Between t = 14τ and 20τ, the contraction of the B-rich network (reflected in the decrease in f_{area}), while its connectivity remains steady (indicated by the plateau in χ_{Euler}), leads to a gradual decrease in f_{loop}. At t = 20τ, the f_{loop} of the $A_{1S}B_{1H}A_{2S}$ system approached the value of the viscoelasticity-symmetric reference system. This evolutionary pathway

https://doi.org/10.1007/s10118-026-3705-7

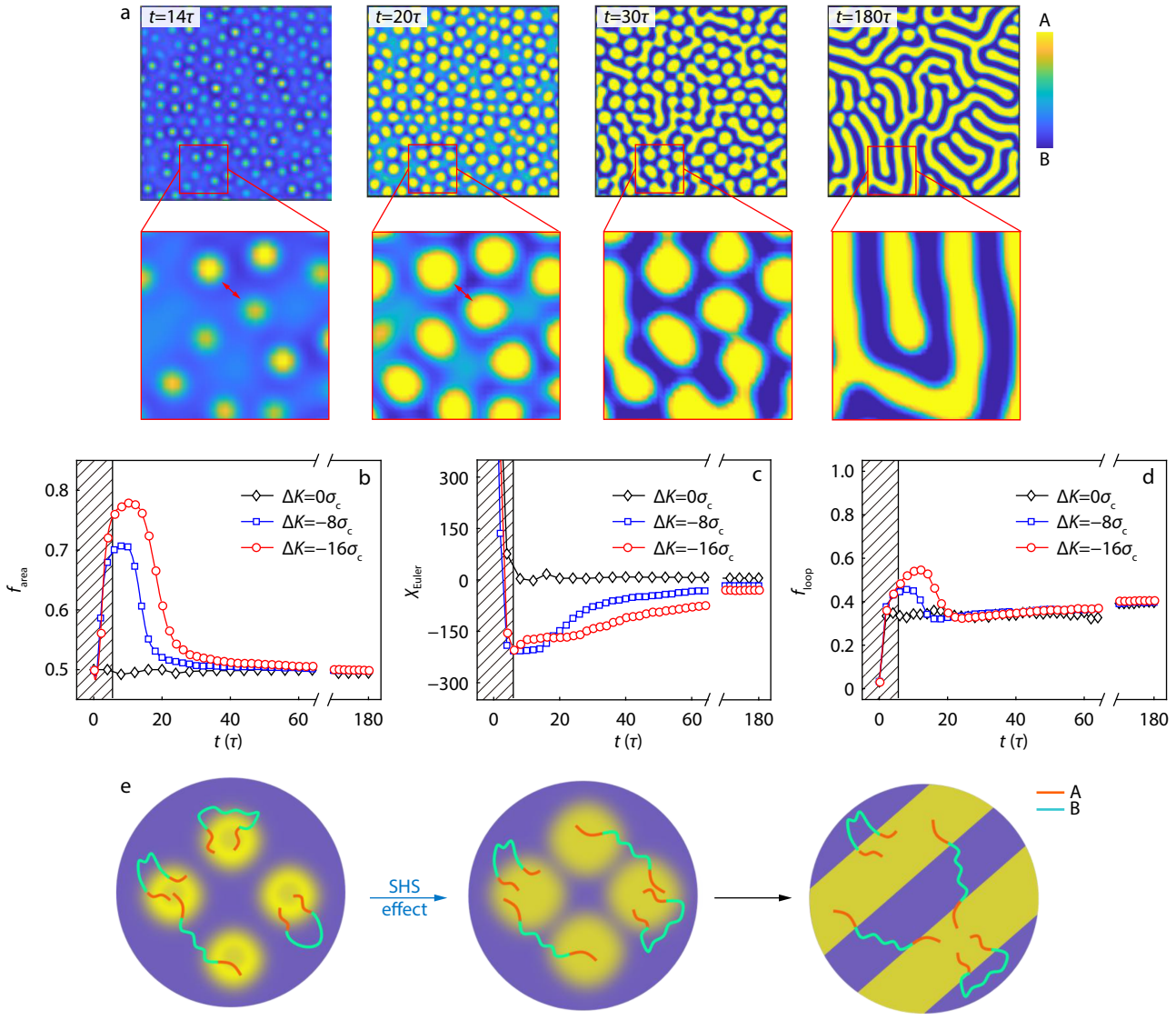

Fig. 3 (a) Morphological evolution of microphase-separated nanostructures of $A_{1S}B_{1H}A_{2S}$ triblock copolymers with higher bulk modulus of inner B_{1H} blocks. The bulk modulus disparity between A and B blocks is set as $\Delta K = K_{A,0} - K_{B,0} = -16\sigma_c$. The double arrows highlight the spatial distance between the droplets. (b) Area fraction f_{area} and (c) Euler characteristic χ_{Euler} of B-rich nanodomains as a function the time t for triblock copolymers with tunable bulk modulus disparity ΔK. The red and green arrows highlight the startups of phase inversion and conformation rearrangement for $\Delta K = -16\sigma_c$. (d) Temporal change in loop probability f_{loop} of B_{1H} blocks. (e) Schematic of mechanistic pathway of soft-hard-soft (SHS) effect during coupled phase inversion and conformation rearrangement. The other representations are the same as those in Fig. 1.

sharply diverges from that of the $A_{1H}B_{1S}A_{2H}$ system. In the latter, f_{loop} remained close to about 1.0, between $t = 14\tau$ and 20τ (Fig. 1d), as the droplets of soft B_{1S} blocks were stably embedded within the continuous network of hard A_{1H} and A_{2H} blocks. However, at $t = 20\tau$, the $A_{1H}B_{1S}A_{2H}$ system underwent a sharp conformational rearrangement, driven by the coalescence of the B-rich droplets.

A mechanistic picture of the VμPS of the $A_{1S}B_{1H}A_{2S}$ triblock copolymer is shown in Fig. 3(e). The process is initiated from a swollen, percolating B-rich network, which corresponds to a moderate initial loop probability. As the thermodynamic force drives the contraction of this network, the spatial support for loop conformations is progressively reduced, leading to a continuous decrease in the loop probability.[83–85] The system eventually evolves into a lamellar morphology, and its conformational distribution converges toward that of the dynamically symmetric case of $\Delta K = 0$. The distinct pathway of a gradual conformational rearrangement driven by network contraction is designated as the soft-hard-soft (SHS) effect, which is distinct from the sharp conformational rearrangement caused by droplet coalescence in the HSH effect of $A_{1H}B_{1S}A_{2H}$ triblock copolymers. Therefore, the viscoelastic sequence of hard and soft blocks acts as a molecular-scale program to direct both the structure and conformation evolution during VμPS.

Effect of Flory-Huggins Interaction Parameter

Building on the finding that the sequence of hard and soft blocks dictates the pathways of microphase separation of block copolymers, we now examine how the thermodynamic driving

force governed by the Flory-Huggins interaction parameter χN modulates their sequence-encoded kinetics. This investigation addresses how the competition between thermodynamics and viscoelasticity influences the conformational evolution of triblock copolymers. Figs. 4(a) and 4(b) show the temporal change of the loop probability f_{loop} of the B blocks under different χN values for the $A_{1H}B_{1S}A_{2H}$ and $A_{1S}B_{1H}A_{2S}$ triblock copolymers, respectively. In both cases, increasing χN from 36 to 44 accelerates microphase separation kinetics and promotes conformational rearrangement of the B blocks, as the enhanced thermodynamic force becomes more effective in resisting viscoelastic suppression of composition fluctuations, thereby inducing earlier and more pronounced conformational changes. In contrast, reducing χN from 36 to 20 delays both microphase separation and the conformational rearrangement of inner blocks because the weaker enthalpic contribution is insufficient to overcome the dominant viscoelastic stresses, which persistently suppress both structure and conformation evolution.

Another key observation is the pronounced influence of χN on the deviation of f_{loop} from the equilibrium value of defect-free lamellae, which is highlighted by dashed lines in Fig. 4. At a high χN, the loop probability f_{loop} exhibits a large deviation from the equilibrium value, whereas at a low χN, it approaches the equilibrium value. This behavior can be explained by the corresponding morphologies of VμPS at various χN values (Figs. 4c and 4d, as well as Fig. S4 in ESI). A high χN results in sharply defined interfaces and defect-rich nanostructures, which kinetically trap the polymer chains in non-equilibrium conformations and retard conformational relaxation. Extended simulations from 400τ to 1200τ confirm that these structures remained metastable for high χN. In contrast, a low χN facilitates defect annihilation, yielding well-defined lamellar domains with near-equilibrium loop conformational characteristics.

We performed additional simulations to examine how end-block asymmetry influences conformation evolution. Keeping the overall composition symmetric (*i.e.*, f_A=f_B=0.50), we varied the composition (f_{A1} and f_{A2}) of the two end blocks in both the HSH- and SHS-type triblock systems with the constraint of $f_{A1} + f_{A2} = 0.50$. Fig. S5 (in ESI) summarizes the effect of end-block asymmetry on the conformation evolution of triblock copolymers during viscoelastic microphase separation. It has been demonstrated that both the HSH and SHS effects remain operative even with asymmetric end blocks. However, asymmetry has the capability to regulate conformational rearrangement in both effects. In particular, the loop probability f_{loop} of the B_{1S} blocks for the asymmetric case of the $A_{1H}B_{1S}A_{2H}$ sequence has a slight increase compared to the symmetric case. It should be noted that the loop probability still evolves toward that of the symmetric system. These phenomena indicate that the fundamental HSH and SHS kinetic motifs are robust to the viscoelastic microphase separation of triblock copolymers, despite end-block asymmetry.

Viscoelastic Microphase Separation of ABAB Tetrablock Copolymers

Turning now to the even-parity system, we investigated $A_1B_1A_2B_2$ tetrablock copolymers, corresponding to the $(AB)_n$ series with $n = 2$. Unlike triblock copolymers, which follow a single evolutionary pathway of the HSH or SHS effect, the alternating sequence of the tetrablock architecture inherently integrates both effects within one chain. Given the constraints of a fixed overall composition (f_A=f_B=0.50) and equal lengths for all blocks (*i.e.*, $f_{A1} = f_{A2}$=f_{B1}=f_{B2}=0.25), this symmetry permits only one sequence under dynamic asymmetry of $\Delta K > 0$: designating A blocks as hard components yields $A_{1H}B_{1S}A_{2H}B_{2S}$ tetrablock copolymers. This unique architecture and sequence establish tetrablock copolymers as a model system for studying the interplay between sequence-specific HSH and SHS effects.

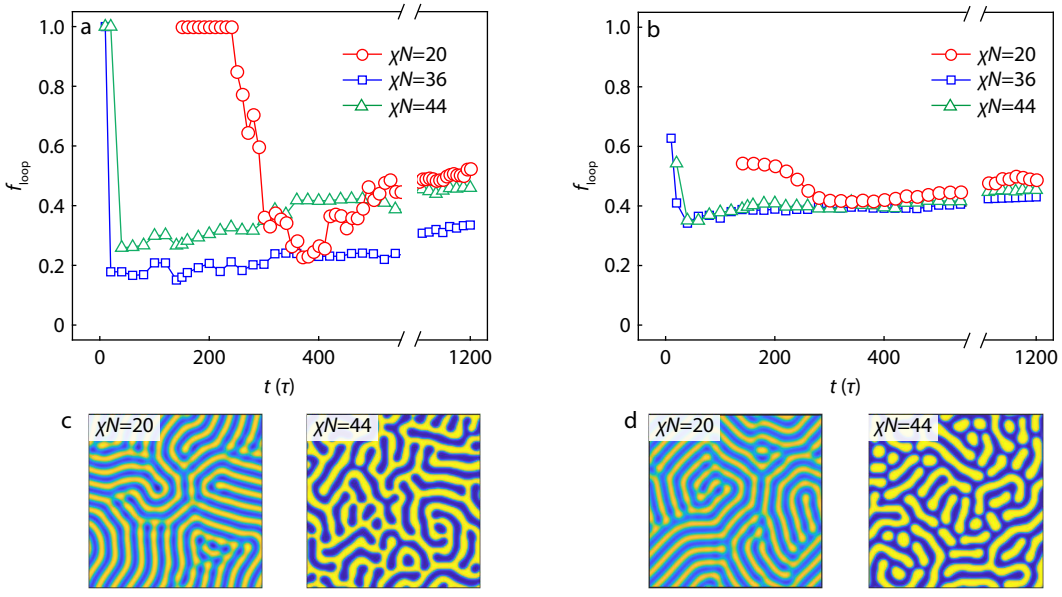

Fig. 4 (a, b) Influence of Flory-Higgins interaction parameter χN on the temporal change of loop probability f_{loop} of B blocks during the viscoelastic microphase separation of (a) $A_{1H}B_{1S}A_{2H}$ and (b) $A_{1S}B_{1H}A_{2S}$ triblock copolymers. Dashed lines highlight the equilibrium value of f_{loop} in defect-free lamellae. (c, d) Microphase-separated morphologies of (c) $A_{1H}B_{1S}A_{2H}$ and (d) $A_{1S}B_{1H}A_{2S}$ triblock copolymers at χN = 20 and 44 at t = 1200τ. The bulk modulus disparity between A and B blocks is set as $|\Delta K|$ = 16.

https://doi.org/10.1007/s10118-026-3705-7

Our DSCFT simulations reveal that the tetrablock copolymers exhibit a phase inversion phenomenon during structural evolution (Fig. S6 in ESI), similar to the triblock copolymer system. However, conformation evolution revealed a complex landscape encoded by an alternating sequence. The $A_{1H}B_{1S}A_{2H}B_{2S}$ chain contained two overlapping triblock-like $A_{1H}B_{1S}A_{2H}$ and $B_{1S}A_{2H}B_{2S}$ sub-chains, each predisposed to different pathways of microphase separation. This design enables concurrent yet distinct conformational pathways within the same molecule, as evidenced by the temporal evolution of loop probabilities for the inner B_{1S} and A_{2H} blocks (Fig. 5a). The A_{2H} blocks within the $B_{1S}A_{2H}B_{2S}$ sub-chains exhibit the characteristic of gradual relaxation within the SHS effect, maintaining a population of mixed loop and bridge conformations. Subsequently, the B_{1S} blocks within the $A_{1H}B_{1S}A_{2H}$ sub-chains exhibit a sharp conformational change in the HSH effect, with the loop probability rapidly changing from high to low values. Thus, the tetrablock copolymers exhibit both HSH and SHS effects within a single molecule, with each effect operating locally within its respective sub-chains.

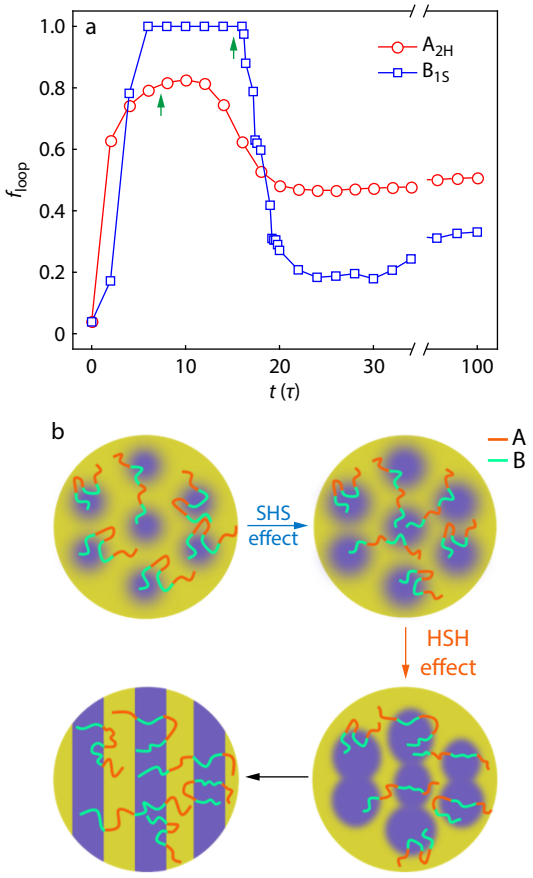

Fig. 5 (a) Temporal change in loop probabilities f_{loop} of B_{1S} and A_{2H} blocks during the viscoelastic microphase separation of $A_{1H}B_{1S}A_{2H}B_{2S}$ tetrablock copolymers. The bulk modulus disparity between A and B blocks is set as $\Delta K = K_{A,0} - K_{B,0} = 16\sigma_c$. The arrows highlight the startups of conformation rearrangement of various sub-chains. (b) Schematic of mechanistic pathway of viscoelastic microphase separation of $A_{1H}B_{1S}A_{2H}B_{2S}$ tetrablock copolymers through hard-soft-hard (HSH) and soft-hard-soft (SHS) effects. The Flory-Huggins interaction parameter is set as $\chi N = 44$.

The synergistic mechanisms of the effects of HSH and SHS are summarized in Fig. 5(b). In the $A_{1H}B_{1S}A_{2H}B_{2S}$ tetrablock copolymers, the dynamic asymmetry initially drives the formation of a percolating network of hard A_{1H} and A_{2H} blocks, within which isolated droplets of soft B_{1S} and B_{2S} blocks are embedded. Within this metastable structure, soft B_{1S} blocks are constrained into loops, whereas A_{2H} blocks adopt a mixed state of loops and bridges. As the system evolves, the cooperative interplay between viscoelastic and thermodynamic forces governs the subsequent pathway. This interplay induces contraction of the A-rich network and triggers the SHS effect, characterized by gradual disengagement of A_{2H} blocks from the loop conformation. Concurrently, the coalescence of the spherical domains of the soft B_{1S} blocks activates the HSH effect, resulting in an abrupt loop-to-bridge conversion of the B_{1S} blocks. This topological reorganization enables the relaxation and bridge formation of both inner blocks, ultimately driving their transformation into a lamellar morphology with a mixed population of loop and bridge conformations.

Thus, the VμPS of ABAB tetrablock copolymers demonstrates sequence-encoded self-assembly kinetics. Unlike the system of triblock copolymers, where the dynamic asymmetry of different blocks yields a single dominant response, the alternating sequence of tetrablock copolymers programs distinct dynamic responses of HSH and SHS effects to concurrently operate within a single molecule. This leads to a temporally coordinated conformational evolution, in which the abrupt change triggered by the HSH effect can couple with the gradual relaxation governed by the SHS effect. These findings confirm that the hard and soft sequences of multiblock copolymers can program multiple relaxation dynamics into one chain, advancing the understanding of non-equilibrium self-assembly beyond the conventional diblock and triblock cases.

Generalizability to Multiblock Copolymers with Extended Sequences

Having established the HSH and SHS effects in ABA triblock copolymers and demonstrated their synergistic operation within a single ABAB tetrablock chain, we proceeded to examine the generalizability of these sequence-encoded self-assembly kinetics to more complex architectures. As the next member of the odd-parity $A(BA)_n$ family, ABABA pentablock copolymers can be used as a prototype system to test whether the sequence-based design principles can be extended to program the conformation kinetics with an increased block number and connectivity. A symmetric pentablock architecture was designed with short outer A blocks (f_{A1}=f_{A3}=0.125) and long inner blocks (f_{A2} = f_{B1} = f_{B2}=0.25) to maintain the global composition symmetry (f_A = f_B=0.50). In a direct analogy to the ABA triblock copolymers, two distinct sequences were constructed by interchanging the positions of hard and soft blocks: one with hard outer and inner A blocks and soft inner B blocks (denoted as $A_{1H}B_{1S}A_{2H}B_{2S}A_{3H}$), and the other with the complementary soft–hard arrangement ($A_{1S}B_{1H}A_{2S}B_{2H}A_{3S}$).

Fig. 6(a) presents the temporal evolution of the loop probabilities for the B_{1S}, A_{2H} and B_{2S} blocks in the $A_{1H}B_{1S}A_{2H}B_{2S}A_{3H}$ pentablock copolymers during VμPS, with the corresponding conformational pathway summarized in Fig. 6(c). The data revealed a competing, yet coordinated evolution of the confor-

https://doi.org/10.1007/s10118-026-3705-7

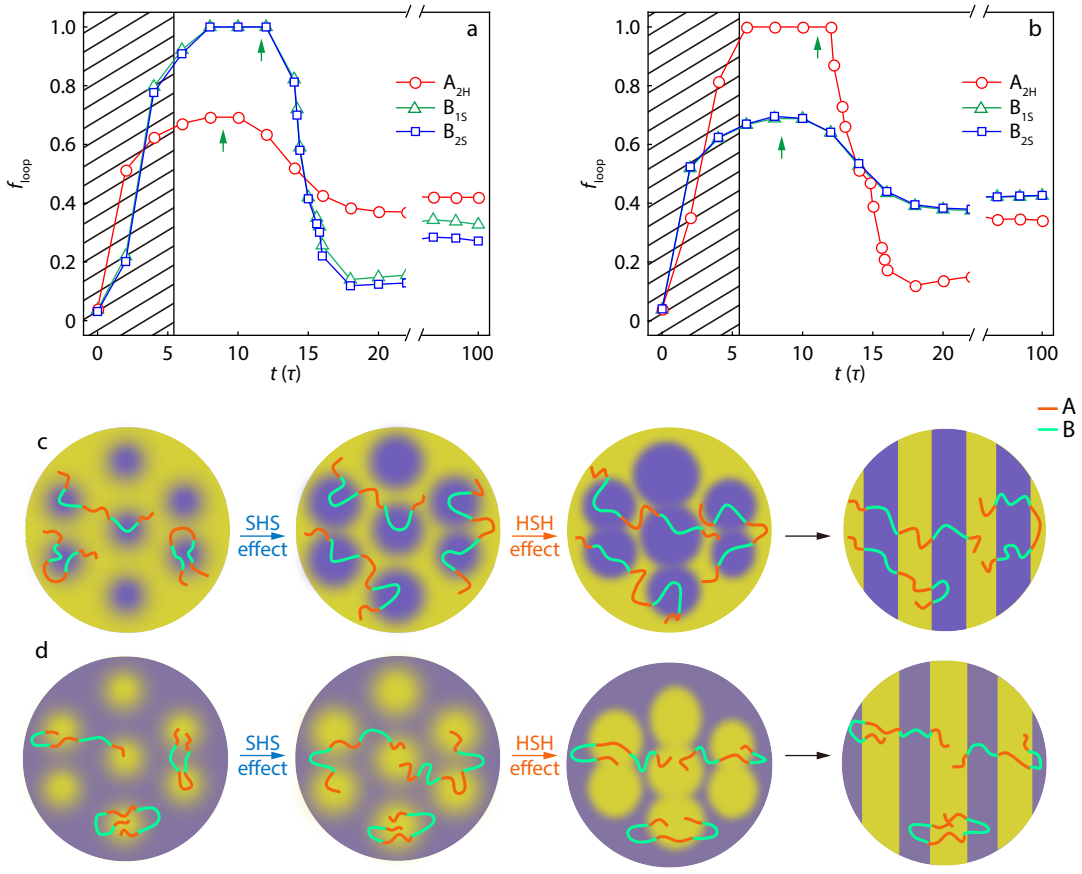

Fig. 6 Conformation evolution and mechanistic pathways of pentablock copolymers during viscoelastic microphase separation. (a) Loop probabilities f_{loop} of B_{1S}, A_{2H} and B_{2S} blocks for $A_{1H}B_{1S}A_{2H}B_{2S}A_{3H}$ sequence at $\Delta K = 16\sigma_c$. The arrows highlight the startups of conformation rearrangement of different sub-chains. (b) Loop probabilities f_{loop} of B_{1H}, A_{2S} and B_{2H} blocks for $A_{1S}B_{1H}A_{2S}B_{2H}A_{3S}$ sequence at $\Delta K = -16\sigma_c$. The Flory-Huggins interaction parameter is set as $\chi N = 60$. (c and d) Schematic of viscoelastic microphase separation pathways mediated by the concurrent HSH and SHS effects for the sequences in (a) and (b).

mation. The hard A_{2H} block first undergoes a gradual loop-to-bridge conformational change under the SHS effect, and subsequently, the soft B_{1S} and B_{2S} blocks experience a sharp change in the loop conformation under the HSH effect. This SHS-HSH hierarchy emerges directly from the embedded and overlapping hard-soft-hard and soft-hard-soft motifs within the chain architecture of pentablock copolymers.

Figs. 6(b) and 6(d) show the conformational evolution of the complementary $A_{1S}B_{1H}A_{2S}B_{2H}A_{3S}$ pentablock copolymers. The kinetic pathway observed here further validates the sequence-encoded framework through a distinct and instructive inversion. The hard B_{1H} and B_{2H} blocks flanked by A blocks undergo a gradual redistribution of their loop conformations—a clear SHS-type response driven by network contraction. Subsequently, the soft, centrally located A_{2S} blocks exhibit a sharp loop-to-bridge change, which is characteristic of the HSH effect triggered by the coalescence of droplet nanodomains. Together, these results demonstrate that the sequence-encoded kinetic framework is generalizable and capable of directing conformational evolution irrespective of sequence permutation or increased architectural complexity.

Following the analysis of odd-parity ABABA pentablock copolymers, we further extended the sequence-encoded kinetic framework to even-parity hexablock copolymers with $A_{1H}B_{1S}A_{2H}B_{2S}A_{3H}B_{3S}$ architecture, corresponding to the $(AB)_3$ case. This architecture possesses an alternating arrangement of both HSH and SHS motifs (*e.g.*, $A_{1H}B_{1S}A_{2H}$ as HSH, followed by $B_{1S}A_{2H}B_{2S}$ as SHS). Fig. 7 shows the loop probabilities of the four inner B_{1S}, A_{2H}, B_{2S} and A_{3H} blocks. The results revealed a localized kinetic picture. The soft B_{1S} and B_{2S} blocks, each embedded within a hard-soft-hard triad, exhibited a sharp decrease in their loop probabilities under the HSH effect. In contrast, the evolution of the hard A_{2H} and A_{3H} blocks exhibited a gradual loop-to-bridge change consistent with SHS-type relaxation. Importantly, although these blocks reside in different long-range sub-chain environments (*e.g.*, as HSH motifs, the B_{1S} block is adjacent to one SHS motif, whereas the B_{2S} block is flanked by two SHS motifs), their conformational evolution is indistinguishable in Fig. 7. This demonstrates unequivocally that conformation evolution is governed by the local HSH or SHS motif, independent of the broader architectural context.

Together, these studies demonstrated that the conformational evolution of complex multiblock chains can be deconstructed into overlapping HSH and SHS kinetic modules. Each module determines the local dynamics of the subchains. The preservation of these motif-specific behaviors with increasing architectural complexity confirmed the robustness, local

https://doi.org/10.1007/s10118-026-3705-7

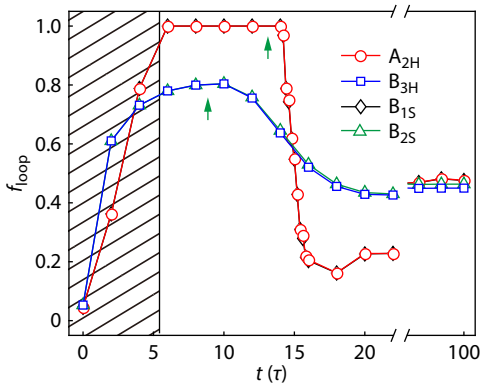

Fig. 7 Temporal change in loop probabilities f_{loop} of B_{1S}, A_{2H}, B_{2S} and A_{3H} blocks during the viscoelastic microphase separation of $A_{1H}B_{1S}A_{2H}B_{2S}A_{3H}B_{3S}$ hexablock copolymers with $\Delta K = 16\sigma_c$. The arrows highlight the startups of conformation rearrangement of different sub-chains. The Flory-Huggins interaction parameter is set as $\chi N = 72$.

determinism, and scalability of the sequence-encoded framework. Therefore, the relaxation pathway of a multiblock chain can be rationally predicted from its motif sequence, thereby establishing a design principle for polymers with programmed hierarchical dynamics.

CONCLUSIONS

In summary, we employed viscoelastic dynamic self-consistent field theory to demonstrate that the linear sequence of hard and soft blocks in multiblock copolymers can act as a molecular-level program to dictate the pathway of conformation evolution during viscoelastic microphase separation. For triblock copolymers, a hard-soft-hard sequence drives a viscoelasticity-driven phase inversion alongside a sharp droplet-coalescence-driven conformation change, whereas a soft-hard-soft sequence leads to a gradual, network-contraction-triggered conformation relaxation. Advancing tetrablock copolymers, we showed that these distinct kinetic effects can be integrated to operate concurrently within a single chain, enabling a temporally coordinated conformation pathway. In addition, this sequence-encoded kinetic framework is generalizable to penta-- and hexa-block architectures, confirming that complex chains can be deconstructed into kinetic modules with predictable behavior. This study establishes that the self-assembly pathway of multiblock copolymers can be programmed through the principle of sequence-encoded viscoelastic kinetics, opening a route for engineering dynamic material properties at the molecular level.

Conflict of Interests

The authors declare no interest conflict.

Electronic Supplementary Information

Electronic supplementary information (ESI) is available free of charge in the online version of this article at https://doi.org/10.1007/s10118-026-3705-7. Details of dynamic self-consistent field theory for multiblock copolymers, schematic illustration of multiblock copolymers, morphological evolution of triblock copolymers with no disparity in bulk moduli, time evolution of thermodynamic and viscoelastic forces, microphase-separated morphologies of triblock copolymers, effect of end-block asymmetry on conformation evolution of triblock copolymers, morphological evolution of tetrablock copolymers are included in ESI.

Data Availability Statement

The simulation data that support the findings of this study are not publicly available but can be obtained from the corresponding author upon reasonable request. The author's contact information: zhangls@ecust.edu.cn (L. Zhang).

ACKNOWLEDGMENTS

This study was financially supported by the National Natural Science Foundation of China (Nos. 22573032 and 22333002) and the Natural Science Foundation of Shanghai (No. 25ZR1401091). The KingFa Company is also acknowledged for their funding.

REFERENCES

1 Brangwynne, C. P.; Eckmann, C. R.; Courson, D. S.; Rybarska, A.; Hoege, C.; Gharakhani, J.; Jülicher, F.; Hyman, A. A. Germline P granules are liquid droplets that localize by controlled dissolution/condensation. *Science* **2009**, *324*, 1729–1732.
2 Hyman, A. A.; Weber, C. A.; Jülicher, F. Liquid-liquid phase separation in biology. *Annu. Rev. Cell Dev. Biol.* **2014**, *30*, 39–58.
3 Shin, Y.; Brangwynne, C. P. Liquid phase condensation in cell physiology and disease. *Science* **2017**, *357*, eaaf4382.
4 Zwicker, D.; Paulin, O. W.; ter Burg, C. Physics of droplet regulation in biological cells. *Rep. Prog. Phys.* **2025**, *88*, 116601.
5 Alberti, S.; Gladfelter, A.; Mittag, T. Considerations and challenges in studying liquid-liquid phase separation and biomolecular condensates. *Cell* **2019**, *176*, 419–434.
6 Dignon, G. L.; Best, R. B.; Mittal, J. Biomolecular phase separation: from molecular driving forces to macroscopic properties. *Annu. Rev. Phys. Chem.* **2020**, *71*, 53–75.
7 Gomes, E.; Shorter, J. The molecular language of membraneless organelles. *J. Biol. Chem.* **2018**, *294*, 7115–7127.
8 Li, P.; Banjade, S.; Cheng, H. C.; Kim, S.; Chen, B.; Guo, L.; Llaguno, M.; Hollingsworth, J. V.; King, D. S.; Banani, S. F.; Russo, P. S.; Jiang, Q. -X; Nixon, B. T.; Rosen, M. K. hase transitions in the assembly of multivalent signalling proteins. *Nature* **2012**, *483*, 336–340.
9 Pappu, R.V.; Cohen, S. R.; Dar, F.; Farag, M.; Kar, M. Phase transitions of associative biomacromolecules. *Chem. Rev.* **2023**, *123*, 8945–8987.
10 Wang, J.; Choi, J.-M.; Holehouse, A. S.; Lee, H.; Zhang, X.; Jahnel, M.; Maharana, S.; Lemaitre, R.; Pozniakovsky, A.; Drechsel, D.; Poser, I.; Pappu, R. V.; Alberti, S.; Hyman, A. A molecular grammar governing the driving forces for phase separation of prion-like rna binding proteins. *Cell* **2018**, *174*, 688–699.
11 Lin, Y.; Protter, D. S. W.; Rosen, M. K.; Parker, R. Formation and maturation of phase-separated liquid droplets by rna-binding proteins. *Mol. Cell* **2015**, *60*, 208–219.
12 Hnisz, D.; Shrinivas, K.; Young, R. A.; Chakraborty, A. K.; Sharp, P. A. Phase separation model for transcriptional control. *Cell* **2017**,

Graphical Abstract

Sequence-encoded Conformation Pathways in Viscoelastic Microphase Separation of Multiblock Copolymers

Zhe-Peng Zhu, Jia-Ping Lin, and Liang-Shun Zhang

East China University of Science and Technology

The sequence-encoded viscoelastic kinetics is introduced to direct non-equilibrium self-assembly pathways of multiblock copolymers and program their distinct conformation evolution, a capability that moves beyond the conventional design of static equilibrium nanostructures.

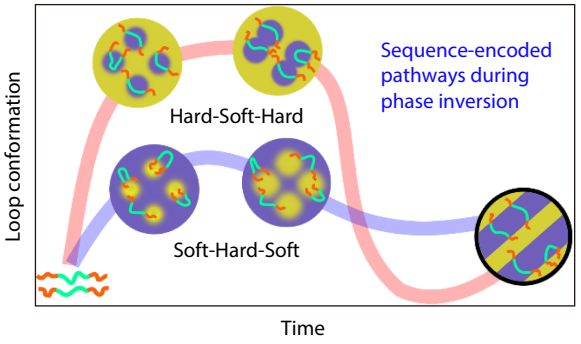

Chinese J. Polym. Sci., 2026 *https://doi.org/10.1007/s10118-026-3705-7*

169, 13–23.
13 Yamazaki, T.; Yamamoto, T.; Yoshino, H.; Souquere, S.; Nakagawa, S.; Pierron, G.; Hirose, T. Paraspeckles are constructed as block copolymer micelles. *EMBO J.* **2021**, *40*, e107270.
14 Choi, J.-M.; Holehouse, A. S.; Pappu, R. V. Physical principles underlying the complex biology of intracellular phase transitions. *Annu. Rev. Biophys.* **2020**, *49*, 107–133
15 Alshareedah, I.; Moosa, M. M.; Banerjee, P. R. Programmable viscoelasticity in protein-rna condensates with disordered sticker-spacer polypeptides. *Nat. Commun.* **2021**, *12*, 6620.
16 Jawerth, L.; Fischer-Friedrich, E.; Saha, S.; Wang, J.; Franzmann, T.; Zhang, X.; Sachweh, J.; Ruer, M.; Ijavi, M.; Saha, S.; Mahamid, J.; Hyman, A. A.; Jülicher, F. Protein condensates as aging maxwell fluids. *Science* **2020**, *370*, 1317–1323.
17 Brady, J. P.; Farber, P. J.; Sekhar, A.; Lin, Y.-H.; Huang, R.; Bah, A.; Nott, T. J.; Chan, H. S.; Baldwin, A. J.; Forman-Kay, J. D.; Kay, L. E. Structural and hydrodynamic properties of an intrinsically disordered region of a germ cell-specific protein on phase separation. *Proc. Natl. Acad. Sci. U. S. A.* **2017**, *114*, E8194–E8203.
18 Espinosa, J. R.; Joseph, J. A.; Sanchez-Burgos, I.; Garaizar, A.; Frenkel, D.; Collepardo-Guevara, R. Liquid network connectivity regulates the stability and composition of biomolecular condensates with many components. *Proc. Natl. Acad. Sci. U. S. A.* **2020**, *117*, 13238–13247.
19 Mittag, T.; Pappu, R. V. A conceptual framework for understanding phase separation and addressing open questions and challenges. *Mol. Cell* **2022**, *82*, 2201–2214.
20 Farag, M.; Cohen, S. R.; Borcherds, W. M.; Bremer, A.; Mittag, T.; Pappu, R. V. Condensates formed by prion-like low-complexity domains have small-world network structures and interfaces defined by expanded conformations. *Nat. Commun.* **2022**, *13*, 7722.
21 Dar, F.; Cohen, S. R.; Mitrea, D. M.; Phillips, A. H.; Nagy, G.; Leite, W. C.; Stanley, C. B.; Choi, J.-M.; Kriwacki, R. W.; Pappu, R. V. Biomolecular condensates form spatially inhomogeneous network fluids. *Nat. Commun.* **2024**, *15*, 3413.
22 Wu, T.; King, M. R.; Qiu, Y.; Farag, M.; Pappu, R. V.; Lew, M. D. Single-fluorogen imaging reveals distinct environmental and structural features of biomolecular condensates. *Nat. Phys.* **2025**, *21*, 778–786.
23 Tejedor, A. R.; Sanchez-Burgos, I.; Estevez-Espinosa, M.; Garaizar, A.; Collepardo-Guevara, R.; Ramirez, J.; Espinosa, J. R. Protein structural transitions critically transform the network connectivity and viscoelasticity of rna-binding protein condensates but rna can prevent it. *Nat Commun* **2022**, *13*, 5717.
24 Lin, Y.; Forman-Kay, J. D.; Chan, H. S. Theories for sequence-dependent phase behaviors of biomolecular condensates. *Biochemistry* **2018**, *57*, 2499–2508.
25 Joseph, J. A.; Reinhardt, A.; Aguirre, A.; Chew, P. Y.; Russell, K. O.; Espinosa, J. R.; Garaizar, A.; Collepardo-Guevara, R. Physics-driven coarse-grained model for biomolecular phase separation with near-quantitative accuracy. *Nat. Comput. Sci.* **2021**, *1*, 732–743.
26 Dignon, G. L.; Zheng, W.; Kim, Y. C.; Best, R. B.; Mittal, J. Sequence determinants of protein phase behavior from a coarse-grained model. *PLoS Comput. Biol.* **2018**, *14*, e1005941.
27 Bates, F. S.; Hillmyer, M. A.; Lodge, T. P.; Bates, C. M.; Delaney, K. T.; Fredrickson, G. H. Multiblock polymers: panacea or pandora's box. *Science* **2012**, *336*, 434–440.
28 Lutz, J. F.; Ouchi, M.; Liu, D. R.; Sawamoto, M. Sequence-controlled polymers. *Science* **2013**, *341*, 1238149.
29 Li, J.; Stayshich, R. M.; Meyer, T. Y. Exploiting sequence to control the hydrolysis behavior of biodegradable plga copolymers. *J. Am. Chem. Soc.* **2011**, *133*, 6910–6913.
30 Matyjaszewski, K. Architecturally complex polymers with controlled heterogeneity. *Science* **2011**, *333*, 1104–1105.
31 Pinheiro, V. B.; Taylor, A. I.; Cozens, C.; Abramov, M.; Renders, M.; Zhang, S.; Chaput, J. C.; Wengel, J.; Peak-Chew, S.-Y.; McLaughlin, S. H.; Herdewijn, P.; Holliger, P. Synthetic genetic polymers capable of heredity and evolution. *Science* **2012**, *336*, 341–344.
32 Lewandowski, B.; De Bo, G.; Ward, J. W.; Papmeyer, M.; Kuschel, S.; Aldegunde, M. J.; Gramlich, P. M. E.; Heckmann, D.; Goldup, S. M.; D'Souza, D. M.; Fernandes, A. E.; Leigh, D. A. Sequence-specific peptide synthesis by an artificial small-molecule machine. *Science* **2013**, *339*, 189–193.
33 Xu, Z.; Dong, Q.; Li, W. Architectural design of block copolymers. *Macromolecules* **2024**, *57*, 1869–1884.
34 Ran, X.; Dong, Q.; Peng, L.; Huang, X.; Li, W. Program asymmetric binary packing lattices of ab1cb2 tetrablock terpolymers. *Macromolecules* **2025**, *58*, 9851–9861.
35 Chen, T.; Xu, Z.; Chu, X.; Peng, L.; Huang, X.; Li, W. A simulation

study on the effect of tailoring molecular architectures on the mechanical behaviors of lamella-forming BABCB linear multiblock copolymers. *Macromolecules* **2025**, *58*, 6387–6398.
36 Chu, X.; Xu, Z.; Cao, Y.; Li, W. Simulation study on the mechanical properties of lamella-forming ABABA linear multiblock copolymers. *Macromolecules* **2024**, *57*, 9536–9545.
37 Schmid, F. Understanding and modeling polymers: the challenge of multiple scales. *ACS Polym. Au* **2023**, *3*, 28–49.
38 Schmid, F.; Li, B. Dynamic self-consistent field approach for studying kinetic processes in multiblock copolymer melts. *Polymers* **2020**, *52*, 2205.
39 Park, S. J.; Myers, T.; Liao, V.; Jayaraman, A. Self-consistent field theory and coarse-grained molecular dynamics simulations of pentablock copolymer melt phase behavior. *Mol. Syst. Des. Eng.* **2024**, *9*, 1235–1253.
40 Lequieu, J.; Quah, T.; Delaney, K. T.; Fredrickson, G. H. Complete photonic band gaps with nonfrustrated ABC bottlebrush block polymers. *ACS Macro Lett.* **2020**, *9*, 1074–1080.
41 Arora, A.; Qin, J.; Morse, D. C.; Delaney, K. T.; Fredrickson, G. H.; Bates, F. S.; Dorfman, K. D. Broadly accessible self-consistent field theory for block polymer materials discovery. *Macromolecules* **2016**, *49*, 4675–4690.
42 Tsai, C. C; Fredrickson, G. H. Using particle swarm optimization and self-consistent field theory to discover globally stable morphologies of block copolymers. *Macromolecules* **2022**, *55*, 5249–5262.
43 Tyler, C. A.; Qin, J.; Bates, F. S.; Morse, D. C. SCFT study of nonfrustrated ABC triblock copolymer melts. *Macromolecules* **2007**, *40*, 4654–4668.
44 Lequieu, J.; Koeper, T.; Delaney, K. T.; Fredrickson, G. H. Extreme deflection of phase boundaries and chain bridging in A(BA′)n miktoarm star polymers. *Macromolecules* **2020**, *53*, 513–522.
45 Subbotin, A.; Klymko, T.; ten Brinke, G. Lamellar-in-lamellar structure of A-B-(B-B-C)$_m$-B-B-A multiblock copolymers. *Macromolecules* **2007**, *40*, 2915–2918.
46 Miglani, C.; Ralhan, J.; Banoo, M.; Nath, D.; Sil, S.; Pal, S. K.; Gautam, U. K.; Pal, A. Stimuli-responsive control over self-assembled nanostructures in sequence-specific functional block copolymers. *ACS Polym. Au* **2024**, *4*, 255–265.
47 MacEwan, S. R.; Weitzhandler, I.; Hoffmann, I.; Genzer, J.; Gradzielski, M.; Chilkoti, A. Phase behavior and self-assembly of perfectly sequence-defined and monodisperse multiblock copolypeptides. *Biomacromolecules* **2017**, *18*, 599–609
48 Roberts, S.; Harmon, T. S.; Schaal, J. L.; Miao, V.; Li, K.; Hunt, A.; Wen, Y.; Oas, T. G.; Collier, J. H.; Pappu R. V.; Chilkoti, A. Injectable tissue integrating networks from recombinant polypeptides with tunable order. *Nat. Mater.* **2018**, *17*, 1154–1163.
49 Dzuricky, M.; Rogers, B. A.; Shahid, A.; Cremer, P. S.; Chilkoti, A. De novo engineering of intracellular condensates using artificial disordered proteins. *Nat. Chem.* **2020**, *12*, 814–825.
50 Choi, J.-W.; Choi, S.-H.; Won, J.-I. Self-assembly behavior of elastin-like polypeptide diblock copolymers containing a charged moiety. *Biomacromolecules* **2021**, *22*, 2604–2613.
51 Patterson, A. L.; Danielsen, S. P. O.; Yu, B.; Davidson, E. C.; Fredrickson, G. H.; Segalman, R. A. Sequence effects on block copolymer self assembly through tuning chain conformation and segregation strength utilizing sequence defined polypeptoids. *Macromolecules* **2019**, *52*, 1277–1286.
52 Khandpur, A. K.; Förster, S.; Bates, F. S.; Hamley, I. W.; Ryan, A. J.; Bras, W.; Almdal, K.; Mortensen, K. Polyisoprene polystyrene diblock copolymer phase diagram near the order-disorder transition. *Macromolecules* **1995**, *28*, 8796–8806.
53 Colby, R. H. Block copolymer dynamics. *Curr. Opin. Colloid Interface Sci.* **1996**, *1*, 454–465.
54 Wu, L.; Cochran, E. W.; Lodge, T. P.; Bates, F. S. Consequences of block number on the order-disorder transition and viscoelastic properties of linear (AB)n multiblock copolymers. *Macromolecules* **2004**, *37*, 3360–3368.
55 Kim, T.; White, J. M.; Bates, F. S.; Lodge, T. P. Universal viscoelastic response of body centered cubic block copolymer solutions: time-temperature-concentration superposition. *Macromolecules* **2025**, *58*, 5579–5589.
56 Lenoch, A.; Schönhoff, M.; Cramer, C. Relaxing, fast and slow: linear viscoelasticity and dynamics in mixed cross-linker metallosupramolecular networks. *Macromolecules* **2024**, *57*, 11507–11519.
57 Tanaka, H.; Araki, T. Phase inversion during viscoelastic phase separation: roles of bulk and shear relaxation moduli. *Phys. Rev. Lett.* **1997**, *78*, 4966–4969.
58 Tanaka, H. Viscoelastic phase separation in biological cells. *Commun. Phys.* **2022**, *5*, 167.
59 Fernández-Rico, C.; Schreiber, S.; Oudich, H.; Lorenz, C.; Sicher, A.; Sai, T.; Bauernfeind, V.; Heyden, S.; Carrara, P.; De Lorenzis, L.; Style, R. W.; Dufresne, E. R. Elastic microphase separation produces robust bicontinuous materials. *Nat. Mater.* **2024**, *23*, 124–130.
60 Huo, Y.; Zhang, H.; Yang, Y. The morphology and dynamics of the viscoelastic microphase separation of diblock copolymers. *Macromolecules* **2003**, *36*, 5383–5391.
61 Yoshimoto, K.; Taniguchi, T. Viscoelastic phase separation model for ternary polymer solutions. *J. Chem. Phys.* **2021**, *154*, 104903.
62 Tanaka, H. Formation of network and cellular structures by viscoelastic phase separation. *Adv. Mater.* **2009**, *21*, 1872–1880.
63 Tanaka, H.; Nishikawa, Y. Viscoelastic phase separation of protein solutions. *Phys. Rev. Lett.* **2005**, *95*, 078103.
64 Shi, W.; Yang, J.; Liu, W.; Zhang, L.; Han C. C. Anomalous phase separation dynamics under asymmetric viscoelastic effect: where fluidic and elastic properties meet. *Macromolecules* **2013**, *46*, 2516–2520.
65 Shi, W.; Chen, F.; Zhang, Y.; Han, C. C. Viscoelastic phase separation and interface assisted crystallization in a highly immiscible ipp/pmma blend. *ACS Macro Lett.* **2012**, *1*, 1086–1089.
66 Tsai, C.-C.; Xu, J.; Duclos, C.; Xie, S. Microstructure and viscoelasticity of oppositely charged ionomer blend melts. *Macromolecules* **2025**, *58*, 1608–1620.
67 Rapp, P. B.; Silverman, B. R. Viscoelastic phase patterning in artificial protein hydrogels. *Macromolecules* **2022**, *55*, 3201–3207.
68 Surendran, A.; Joy, J.; Parameswaranpillai, J.; Anas, S.; Thomas, S. An overview of viscoelastic phase separation in epoxy based blends. *Soft Matter* **2020**, *16*, 3363–3377.
69 Jose, J.; Joseph, K.; Pionteck, J.; Thomas, S. Pvt behavior of thermoplastic poly(styrene-co-acrylonitrile)-modified epoxy systems: relating polymerization-induced viscoelastic phase separation with the cure shrinkage performance. *J. Phys. Chem. B* **2008**, *112*, 14793–14803.
70 Zhu, Z.; Lin, J.; Zhang, L. Breaking composition constraints: viscoelasticity-driven phase inversion for mechanically robust block copolymer networks. *Macromolecules* **2026**, *59*, 312–325.
71 Müller, M.; Schmid, F. Incorporating fluctuations and dynamics in self-consistent field theories for polymer blends. *Adv. Polym. Sci.* **2005**, *185*, 1–58.
72 Fraaije, J. G. E. M.; Vlimmeren, B. A. C.; Maurits, N. M.; Postma, M.; Evers, O. A.; Hoffmann, C.; Altevogt, P.; Goldbeck–Wood, G. The dynamic mean-field density functional method and its application to the mesoscopic dynamics of quenched block copolymer melts. *J. Chem. Phys.* **1997**, *106*, 4260–4269.
73 Zhang, L.; Sevink, A.; Schmid, F. Hybrid lattice boltzmann/dynamic self-consistent field simulations of

microphase separation and vesicle formation in block copolymer systems. *Macromolecules* **2011**, *44*, 9434−9447.
74 Doi, M.; Onuki, A. Dynamic coupling between stress and composition in polymer solutions and blends. *J. Phys. II France* **1992**, *2*, 1631-1656.
75 Hall, D. M.; Lookman, T.; Fredrickson, G. H.; Banerjee, S. Hydrodynamic self-consistent field theory for inhomogeneous polymer melts. *Phys. Rev. Lett.* **2006**, *97*, 114501.
76 Fredrickson, G. H. *The equilibrium theory of inhomogeneous polymers*; Oxford University Press: New York, **2013**.
77 Tanaka, H. Viscoelastic model of phase separation. *Phys. Rev. E* 1997, *56*, 4451−4462.
78 Hall, D. M.; Lookman, T.; Fredrickson, G. H.; Banerjee, S. Numerical method for hydrodynamic transport of inhomogeneous polymer melts. *J. Comput. Phys.* **2007**, *224*, 681−698.
79 Matsen, M. W.; Thompson, R. B. Equilibrium behavior of symmetric aba triblock copolymer melts. *J. Chem. Phys.* **1999**, *111*, 7139−7146.
80 Drolet, F.; Fredrickson, G. H. Optimizing chain bridging in complex block copolymers. *Macromolecules* **2001**, *34*, 5317−5324.
81 Zhang, L.; Lin, J.; Lin, S. Morphologies and bridging properties of graft copolymers. *J. Phys. Chem. B* **2007**, *111*, 351−357.
82 Araki, T.; Tanaka, H. Three-dimensional numerical simulations of viscoelastic phase separation: morphological characteristics. *Macromolecules* **2001**, *34*, 1953−1963.
83 White, J. M.; Kim, T.; Bates, F. S.; Lodge, T. P. How does the rate of chain exchange relate to stress relaxation in triblock copolymer networks. *ACS Cent. Sci.* **2025**, *11*, 422−430.
84 Kim, T.; White, J. M.; Magruder, B. R.; Danielson, E.; Bates, F. S.; Lodge, T. P. Concentration-driven slowdown of chain-exchange kinetics in block copolymer micelle solutions. *Macromolecules* **2025**, *58*, 10580−10590.
85 Prhashanna, A.; Dormidontova, E. E. Micelle self-assembly and chain exchange kinetics of tadpole block copolymers with a cyclic corona block. *Macromolecules* **2020**, *53*, 982−991.

https://doi.org/10.1007/s10118-026-3705-7